JOURNAL OF SPACECRAFT AND ROCKETS
Vol. 47, No. 5, September–October 2010

Simulating Nonequilibrium Flow for Ablative Earth Reentry

J. S. Shang*
Wright State University, Dayton, Ohio 45435
and
S. T. Surzhikov†
Russian Academy of Sciences, 119526, Moscow, Russia

DOI: 10.2514/1.49923

The present study of kinetic models for hypersonic nonequilibrium flow attempts to better understand the vibrational relaxation by comparing Park's model and the preferential dissociation formulations of Treanor–Marrone. A simplified approximation for conductive–convective heat transfer computation on the Stardust capsule has also been implemented by recognizing that the electron excitation rarely populates beyond first quantum level above ground state. In addition, the partially ionized gas is in a global neutrality condition; as a consequence, the electrostatic force and work done by charged particles is negligible in the absence of an externally applied electromagnetic field. Therefore, it may be of a limited value for solving the electronic energy conservative equation for conductive and convective heat transfer. Numerical simulations by suppressing this equation in the present effort have supported this observation. Finally, a spectral group approach for analyzing nonequilibrium radiation heat transfer is also presented to complete the description of hypersonic nonequilibrium flow.

Nomenclature

$\mathbf{B}$	=	magnetic field intensity, Wb/m^2
d	=	coefficient of drift velocity, m^2/sV
$\mathbf{E}$	=	electrical field intensity, V/m
e	=	specific internal energy, J/kg
h	=	specific enthalpy, J/kg
$\mathbf{I}$	=	identity matrix
$\mathbf{J}$	=	electrical current density, A/m^2
$\mathbf{J}_\omega$	=	spectral intensity of radiation, W/m^{2}s
M	=	molecular weight, kg/mol
p	=	static pressure, N/m^2
Q	=	energy transfer among internal degrees of freedom, W/kg
r	=	radius of spherical coordinate, m
T	=	temperature, K
$\mathbf{u}$	=	velocity vector, m/s
w	=	net product of chemical species, mol/s
κ_ω	=	spectral absorption coefficient, W/m^{2}srad
μ	=	diffusion coefficient, m^2/s
ν	=	stoichiometric coefficient
ρ	=	density, kg/m^3
$\boldsymbol{\tau}$	=	molecular shear stress tensor, N/m^2
Ω	=	solid angle, rad

Subscripts

e	=	electronic excitation state
i	=	individual chemical species
v	=	vibrational excitation state

Presented as Paper 2010-983 at the 48th AIAA Aerospace Sciences Meeting, Orlando, FL, 4–7 January 2010; received 17 March 2010; revision received 16 April 2010; accepted for publication 13 May 2010.

*Department of Mechanical and Materials Engineering; joseph.shang@wright.edu.
†Radiative Gasdynamics Laboratory.

Introduction

THE challenge in analyzing the ablation phenomenon arises from the complex interdisciplinary nature. In spite of extensive applications of ablators for thermal protection during the past decades, the physical-chemical process of ablating in the reentry environment is still not fully understood [1–4]. Furthermore, the most widely adopted phenolic impregnated carbon ablator is frequently reinforced by secondary impregnation of polymethyl methacrylate to maximize the pyrolysis gas generation so to minimize the char surface recession [2]. All these added physical-chemical phenomena always occur at the atomic or molecular scales that can be only modeled by computational simulation [3,4]. The accuracy of the ablation model based upon a limited experimental database and under the harsh environment is severely limited in physical fidelity. The nonequilibrium aerodynamic and thermodynamic state in which the ablation takes place is equally daunting.

The kinetic energy of any reentry vehicle has to convert and to dissipate in the form of thermal energy when entering the atmosphere of the Earth [5]. A part of the energy is deposited on the surface of the reentry vehicle. Depending on the reentry speed, the heat transfer rate varies widely from a low-Earth-orbital reentry speed of 8 km/s to Galileo reentry speed up to 47.7 km/s; the rate span is a range from 2.3×10^2 to 1.7×10^5 kW/m^2 [6]. Under this condition, nonequilibrium thermodynamic state and chemical reactions are the common features of the reentry hypersonic flows. The intensive interaction of high-temperature gas and surface material is clearly in evidence. Intriguing ablation patterns have been found on the recovered reentry vehicle and meteorites and it has been studied for decades. However, for the purpose of thermal protection, the current interests are focused on the recession rate of ablating material. Therefore, the investigations of known physical-chemical kinetic models for physical fidelity and computational efficiency have been sustained.

The nonequilibrium chemical and thermodynamic flow is investigated by using the conservation laws of interdisciplinary computational fluid dynamics for high-temperature gas. On the framework of continuum mechanics, the bridge linking Boltzmann equation and conservative laws of aerodynamics is the kinetics theory of gas and Chapman–Enskog expansion [7]. Since the kinetic theory does not consider the internal structure of atom and molecule, the higher degrees of excitation beyond the translation motion must be resolved by approximations. Traditionally, the connection between molecular and atomic structures and thermodynamic behavior of high-temperature gas is described by statistic mechanics and

augmented by knowledge from quantum physics. The calculation of finite rate chemical reaction including carbonaceous ablating surface often adopts the chemical kinetic models either by Park [8] or Zhluktov and Abe [9]. A huge amount of research results have been derived from this approach and, more recently, even extended to include the ablation phenomenon [1,2,10]. However, a significant discrepancy has been noted for this group of results from the limited amount of flight data. A part of the discrepancy is due to inaccurate computation or inadequate measurement technique, but a major portion of this disparity is incurred by the analytical modeling [11,12].

In most chemical-physical kinetic models, the remarkable correlation for vibration relaxation by Millikan and White [13] has been widely adopted. They have found that at a given ambient pressure, a linear relationship exists between the logarithmic relaxation time scale and the inverse one-third power of system temperature, $\log(p\tau_v) \approx CT^{-1/3}$. Indeed, their correlation accurately describes the vibrational relaxation rates for a wide range of gas species. Meanwhile, they also point out that at a sufficiently high-temperature condition for dissociation to occur, this vibrational relaxation time scale with the competing process may not be physically meaningful [13]. To address this issue, Treanor and Marrone have specifically developed a coupled vibration–dissociation (CVD) model [14], which will be explicitly implemented in the present numerical simulation.

At the altitude of 81.6 km, the Stardust capsule attained the reentry speed to Earth of 12.6 km/s, which is the fastest speed of man-made objects [15]. Under this condition, the maximum temperature behind the bow shock has a predicted range from 24,000 to 58,680 K and rapidly expanding toward downstream [16,17]. This value has reached and exceeded the electronic characteristic temperatures of excited quanta above ground state for some gas species. However, judging from the numbers of collisions required for energy transfer, the highly excited quantum level may not be densely populated. The major portion of the energy transfer to the electronic excitation thus could be adequately described by the chemical kinetic process alone. Furthermore, in the absence of an externally applied electromagnetic field, the electrostatic force, Lorentz acceleration, and Joule heating in globally neutral plasma vanish. Again in the absence of an externally applied electric field, the diffusion and the ambipolar diffusion becomes the principal mechanism for the charged-particle motion. In fact, the ordinary diffusion has been appropriately taken into account by the kinetic theory for transport property. As a consequence, the electromagnetic forces and the work done by the charged species cease, which may render the electron energy conservation equation unnecessary for calculating conductive and convective heat transfer. This assertion becomes another objective of the present effort.

In the hypersonic reentry environment, the radiation heat transfer generates a substantial amount of energy transfer in addition to the convective and conductive processes. In fact, at the maximum heat loading condition of the Stardust reentry, the typically predicted radiation heat transfer rate is 120 w/cm^2 versus the conductive–convective heat transfer rate of 839 w/cm^2 [16,17]. Therefore, it becomes critically important to understand the basic mechanism and to develop accurate predictive methods for nonequilibrium radiative heat transfer.

As a prerequisite for ablation research, the present effort is concentrated on an examination of current physical-chemical kinetic models for physical fidelity and computational efficiency. The main emphasis is focused on the interaction of the internal degrees of freedom of high-temperature gas mixture. For this reason, computational results from a previous study of the RAM-C-II probe and the Stardust sample return capsule from the present simulation are analyzed together. At the same time, a preliminary effort is also devoted to develop a procedure for analyzing the nonequilibrium radiation heat transfer using spectral grouping approach [18].

Governing Equations

In numerical simulation, accurate prescription of the interface boundary conditions of mass, momentum, and energy balance are required and they are strongly dependent on the ambient condition. In fact, some of the critical chemical reactions of the ablative material are exclusively determined by the components of the surrounding high-temperature air mixture [10,11]. Therefore, a detailed knowledge of the gas composition in the nonequilibrium shock layer and the physically meaningful interface boundary conditions are paramount in describing the ablation phenomenon and will be the focus of the present investigation.

The detailed mechanisms for nonequilibrium reacting gas are developed from gas kinetic models. The conservation equations in continuum medium can be given as [16,19,20]

$$\frac{\partial \rho_i}{\partial t} + \nabla \cdot [\rho_i(\mathbf{u} + \mathbf{u}_i)] = \frac{\mathrm{d}w_i}{\mathrm{d}t} \tag{1}$$

$$\frac{\partial \rho u}{\partial t} + \nabla \cdot (\rho \mathbf{u}\mathbf{u} + p\mathbf{I} - \boldsymbol{\tau}) = \rho_e \mathbf{E} + (\mathbf{J} \times \mathbf{B}) \tag{2}$$

$$\frac{\partial \rho e}{\partial t} + \nabla \cdot \left[\rho e \mathbf{u} - \kappa \nabla T + \sum \rho_i u_i h_i + q_{\mathrm{rad}} + \mathbf{u} \cdot p\mathbf{I} + \mathbf{u} \cdot \boldsymbol{\tau} \right] + Q_{vt} - Q_{et} = \mathbf{E} \cdot \mathbf{J} \tag{3}$$

The vibrational energy conservation equations for polyatomic molecular species are

$$\frac{\partial \rho_i e_{iv}}{\partial t} + \nabla \cdot [\rho_i(\mathbf{u} + \mathbf{u}_i)e_{iv} + q_{iv})] = e_{iv} \frac{\mathrm{d}w_i}{\mathrm{d}t} + Q_{v,\Sigma} \tag{4}$$

The electronic energy conservation equation has been traditionally given as

$$\frac{\partial \rho_i e_e}{\partial t} + \nabla \cdot [\rho_i(\mathbf{u} + \mathbf{u}_i)e_e + \mathbf{u} \cdot p_e\mathbf{I} + q_e)] = e_e \frac{\mathrm{d}w_i}{\mathrm{d}t} + \mathbf{E} \cdot \mathbf{J} + [\rho_e \mathbf{E} + (\mathbf{J} \times \mathbf{B})] \cdot (\mathbf{u} + \mathbf{u}_i) + Q_{e,\Sigma} \tag{5}$$

where $\mathbf{J}$ is the current density of the partially ionized gas,

$$\mathbf{J} = e[-d_i \nabla n_i + d_e \nabla n_e + (n_i \mu_i + n_e \mu_e)\mathbf{E}]$$

in which the diffusion and drift velocity of both ions and electrons are included. The vector fields of $\mathbf{E}$ and $\mathbf{B}$ are the sum of the externally applied and induced electrical and magnetic field intensities. In the absence of either an externally applied electrical and magnetic field, the induced electromagnetic field intensity is negligible in comparison with the aerodynamic inertia. Therefore, the effects of the electromagnetic force and the work done to the gas mixture shall be extremely limited. However, the electrically conducting medium has a pronounced effect on the electromagnetic wave propagation. The relative frequencies of the partially ionized plasma and the radio communication have led to the well-known communication blackout phenomenon.

The net energy transfer between translational, vibrational, and electronic excitations and the sums in each degree of freedom that appear in Eq. (5) are designated as Q_{vt}, Q_{et}, $Q_{v,\Sigma}$, and $Q_{e,\Sigma}$, respectively. A wide range of plausible models has been proposed and implemented with impunity through insights, but with a limited database for validation to become a critical area for intensive research [8–14,16–25]. Specifically, the electronic kinetic models of electron impact ionization and associative ionization have not been modeled on physical understanding. These chemical-physical processes are characterized by multistage interactions and have been overlooked [18]. This subject will remain as a sustained research focus for the present effort into the future and will also extend further to include the ablation.

The rate of the species generation and depletion is described by the Arrhenius equation based on the law of mass action [26]:

$$\frac{\mathrm{d}w_i}{\mathrm{d}t} = M_i \sum_{j=1}^{J} (\nu''_{i,j} - \nu'_{i,j}) \left\{ K_{f,j} \prod_{k=1}^{N_{kf}} \left(\frac{\rho_k}{M_k} \right)^{\nu'_{k,j}} - K_{b,j} \prod_{k=1}^{N_{kb}} \left(\frac{\rho_k}{M_k} \right)^{\nu''_{k,j}} \right\} \tag{6}$$

For the present investigation, the forward and backward chemical-reaction-rate constants are adopted from the works of Olynick et al. [16] and Park [17].

The definition of the internal energy is now given as

$$\rho e = \sum_{i \neq e} \rho_i \left(c_{v,i} T + \frac{\mathbf{u} \cdot \mathbf{u}}{2} \right) + \sum_{i \neq e} \rho_e e_{v,i} + \sum_{i \neq e} \rho_i h_i^o + \rho_e \left(c_{v,e} T_e + \frac{\mathbf{u}_e \cdot \mathbf{u}_e}{2} \right) \tag{7}$$

where h_i^o is the standard heat of formation for all reacting species. When an externally applied electrical field is absent, the electron drift velocity vanishes. The driven mechanism for the charged-particle motion is solely derived from the diffusion; thus, the electron velocity can be calculated from Fick's law, like all neutral species in a high-temperature gas mixture [21–24,26].

For the nonequilibrium hypersonic flow over a blunt body, the appropriate initial values and boundary conditions have been established [8,9,17]. The only implicit assumption for the species conservation equations at the surface is either noncatalytic or fully catalytic. However, the mostly widely used condition is to simply let the chemical-reaction controls by the local thermodynamic condition be identical to the interior domain of the shock layer [16–20]; technically, it is assumed that the solid surface is fully catalytic. On the ablating surface, the interface boundary conditions are much more complex than the initial values. The latter can be accurately described by the nonequilibrium high-temperature air composition in the shock layer and will be discussed in the subsequent section.

For describing the ablating surface, the majority of research efforts have been concentrated on the interface boundary conditions, either from physical observations or by unique insights [1,2,6,10–12,16–25]. In theory, the interface boundary condition can be rigorously derived from the governing equations on the surface of the control volume. These interface conditions can be summarized as follows:

For species conservation equations,

$$[\rho_+ c_{i+} (\mathbf{u}_+ + \mathbf{u}_{+i} - u_{b+}) - \rho_- c_{i-} (\mathbf{u}_- + \mathbf{u}_{-i} - \mathbf{u}_{b-})] \cdot n_+ A = \lim_{v \to 0} \left[\iiint w_i \, \mathrm{d}V - \frac{\mathrm{d}}{\mathrm{d}t} \iiint \rho c_i \, \mathrm{d}V \right] \to 0 \tag{8}$$

For momentum conservation equations,

$$[\rho_+ \mathbf{u}_+ (\mathbf{u}_+ - \mathbf{u}_{b+}) - \rho_- \mathbf{u}_- (\mathbf{u}_- - \mathbf{u}_{b-}) - (\tilde{\sigma}_+ - \tilde{\sigma}_-)] \cdot n_+ A = \lim_{v \to 0} \left[\iiint \rho \sum_{i=1}^{n} c_i \mathbf{f}_i \, \mathrm{d}V - \frac{\mathrm{d}}{\mathrm{d}t} \iiint \rho \mathbf{u} \, \mathrm{d}V \right] \to 0 \tag{9}$$

For internal energy conservation equations,

$$[\rho_+ e_+ (\mathbf{u}_+ - \mathbf{u}_{b+}) - \rho_- e_- (\mathbf{u}_- - \mathbf{u}_{b-}) + \mathbf{q}_+ - \mathbf{q}_- - \mathbf{u}_+ \cdot \tilde{\sigma}_+ + \mathbf{u}_- \cdot \tilde{\sigma}_-] \cdot n_+ A = \lim_{v \to 0} \left[\iiint \dot{q} \, \mathrm{d}V + \iiint \rho \sum_{i=1}^{n} c_i \mathbf{f}_i \cdot (\mathbf{u} + \mathbf{u}_i) \, \mathrm{d}V - \frac{\mathrm{d}}{\mathrm{d}t} \iiint \rho e \, \mathrm{d}V \right] \to 0 \tag{10}$$

In the above equations, the subscript symbols + and − denote the variables evaluated above or beneath the ablating interface and thus separate the required descriptions for the nonequilibrium gas from the ablator. The velocity of the recessing surface is indicated as u_b, which is permitted to vary from point to point on the control surface. In this formulation, the ejection velocity of pyrolysis gas and the release vapor rate of the sublimated material on the ablating surface are required. Therefore, the detailed mechanisms of gaseous motion through the porous ablating material are relegated to the research results of ablative material. The heat transfer term q accommodates the heat flux by conduction, convection, and radiation transfer according to the energy conservation equation (3). Finally, the normal stress component is designated as $\tilde{\sigma}$ and it is the only tensoral stress component that can contribute to the work done by the gas media: the nonequilibrium gas, sublimating vapor, and pyrolysis gas of the ablating material.

The present formulation is derived from the structure of the governing equations and has the direct link to the eigenvector of the partial differential equations system. This result intends to show these interface boundary conditions are much more complex for an ablating surface in the existing literatures. Addition efforts are still required as to how these conditions can be implemented and ensured to maintain the computational stability. At the present time, it has not been verified completely that the interface boundary condition can satisfy the well-posed criterion for numerical simulation. This is another sustained research objective of the present effort.

Numerical Procedure

The system of complex governing equations including aerodynamic and nonequilibrium chemical reactions are loosely coupled, but a uniform convergence criterion of the relative error is maintained for all numerical results on the order of magnitude of 10^{-5}. The interdisciplinary aerodynamic equations (equations for momentum transfer) were solved by a low-diffusion flux-splitting method through the time-derivative preconditioning to eliminate the numerical limiters [27]. This approach is especially effective in the shock layer, where the speed of sound is no longer to be an important scale for flux vector at the cell interface. The energy and species conservation equations are integrated by the implicit finite difference scheme of the second-order accuracy in space and time. The numerical stability for these two groups of conservation equations can be easily maintained by treating the convective and diffusive terms by windward and central approximations. The additional details of the adopted numerical procedures can be found in the work of Surzhikov and Shang [21].

To be consistent with the kinetic model of internal structure of gas, transport properties of the gas mixture for thermal diffusion, viscosity, and thermoconductivity are calculated from Boltzmann equation by Chapman–Enskog expansion [7]. All collision integrals and cross sections are obtained from either the Lenard-Jones potential for nonpolar molecules or a polarizability model for ion-neutral nonresonant collisions by Capitelli et al. [28] and Levin and Wright [29] and augmented by the results by Svehla [30]. The kinetic theory also gives the viscosity and thermal conductivity for gas mixture; these formulas are also known as Wilke's mixed rule [31].

Two numerical simulations were performed for the RAM-C-II probe [32] and the Stardust sample return capsule [15]. The former has a basic configuration of a spherical cone with a nose radius of 15.24 cm and a semiconical angle of 9 deg. The overall length of the vehicle is 129.54 cm. The flight-test data were collected at the altitudes from 53.3 to 85.3 km and at flight speed of 7.62 m/s with a small angle of attack. Therefore, a simple grid of 51 × 105 with the C topology is sufficient for the present purpose.

On the other hand, the Stardust reentry configuration consists of a 60 deg one-half-angle spherical cone with a nose radius of 0.229 m as the forebody. The afterbody is a truncated 30 deg cone with a base radius of 0.406 m. The corner radius of this configuration at the juncture of the forebody and afterbody is merely 0.02 m. The freestream conditions at the reentry velocity of 11.137 km/s for the present simulation can be summarized as follows: the air density air is 2.34×10^{-4} kg/m^3 and the ambient temperature is 238 K. In the initial research phase, the entire flowfield is constructed by a composite of three contiguous domains. The near-body flowfield is described by two grid systems matched at the corner for the upstream and the near-wake region. The far-field domain is also contiguously connected to the near-wake mesh system, and the mesh is highly stretched toward the far field downstream. For the present purpose,

the simulation is restricted to the axisymmetric approximation. The initial computational grid systems of the upper-half symmetric plane have the dimensions of 31×41, 31×41, and 21×41.

Most computational results are generated on a refined grid system with four grid blocks; each consists of a 41×71 grid to facilitate concurrent computing. The finest grid spacing of 0.01 cm is located immediately adjacent to the surface of the Stardust probe. Figure 1 depicts the entire flowfield in a composite presentation of Mach number contours, streamline trace, and supporting grid. The finite rate chemical kinetic model for nonequilibrium air is used to establish the initial values for the ablation investigation [12]. After that, two chemical kinetic models by Olynick et al. [16] and Park [17] for chemical reaction with carbonaceous surface were compared first and selectively applied later. The transport properties of the ablating gas mixture are consistently calculated by the collision integrals [28–30] through the kinetic theory and Wilke's mixing rule [7,31]. The attached strong bow shock and the rapid expansion around the corner of the forebody are accurately captured by the numerical simulation. The separated flow that appears as the recirculating region by the axisymmetric approximation is also revealed in the near-wake region immediately adjacent to the base of the capsule. The secondary feature, such as the neck of the near wake after the recompression, is also exhibited. However, there are indications at the multiblock interfaces, some grid refinement and topology structure improvement may still be desired. In any event, all critical aerodynamic phenomena are reasonably duplicated.

The species concentration in particle number density along the stagnation streamline is presented in Fig. 2. From this presentation, the bow shock standoff distance is found at 1 cm upstream from the stagnation point of the Stardust capsule. The nitrogen atoms have the highest and a nearly uniform number density within the shock layer to attain a value of 1.0×10^{17} per cubic centimeter. However, the atomic nitrogen recombines at the catalytic surface and yields a high number density of 4.8×10^{17} per cubic centimeter for the molecular nitrogen. The number of electrons increases rapidly downstream from the bow shock and reaches a maximum value of 7.0×10^{15} and then diminishes quickly toward the capsule surface. The profile of the positively charged nitrogen atoms, which is the dominant component of the ions follows the behavior of the electrons closely. By summing all number density of the positive charged species (N^+, O^+, NO^+, N_2^+, and O_2^+), the global neutrality of a partially ionized plasma is unmistakable displayed. Therefore, one may conclude that the electrostatic force due to space charge separation and Joule heating appeared in the second and third terms in the right-hand side of Eq. (5) vanishes.

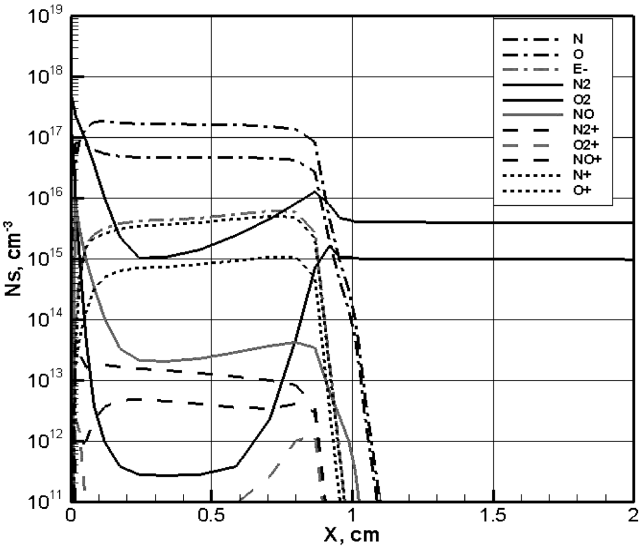

Fig. 2 Species concentrations along the stagnation streamline of the Stardust capsule; $u_\infty = 11.137$ km/s.

Figure 3 depicts the molar fractions of atomic nitrogen and oxygen within the shock envelope of the Stardust probe. A high concentration of atomic nitrogen is observed in the stagnation region and extends to the outer edge of the heat shield. It becomes obvious that the nitridation is an important chemical reaction over the entire heat shield and has a profound effect on the mass blowing rate, as well as heat flux across the interface of the ablator. Therefore, any chemical kinetic model does not include nitridation underpredicts the mass blowing rate in the stagnation region where the dissociated nitrogen has a significant concentration [2,9]. In contrast, there is no significant presence of oxygen atoms adjacent to the ablative surface; the oxidation of carbon in the solid phase may have a limited effect on the ablation prediction. These important observations were first made by Chen and Milos [2] in their study on the thermal response of spacecraft heat shield for ablation phenomena [2].

For ablation simulation, two major contributions of heat transfer by conductive and convective mechanisms to the body surface are important. In the present investigation, both the chemical kinetic models by Olynick et al. [16] and Park [17] for carbonaceous surface are adopted interchangeably. A typical surface heat transfer distribution using Park's model along the capsule symmetric plane is

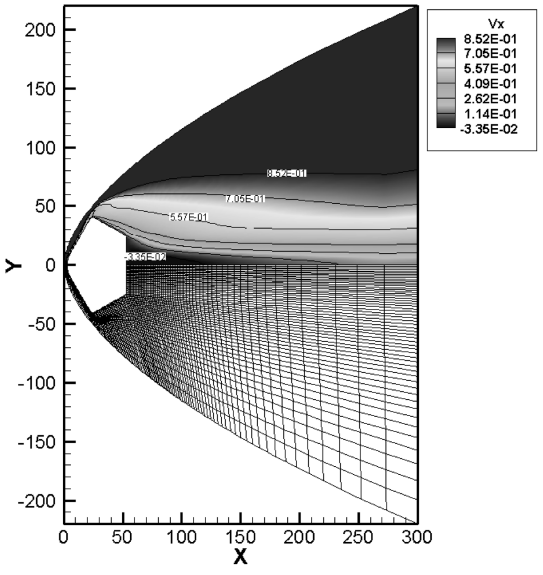

Fig. 1 Grid topology and velocity field around the Stardust configuration; $u_\infty = 11.137$ km/s.

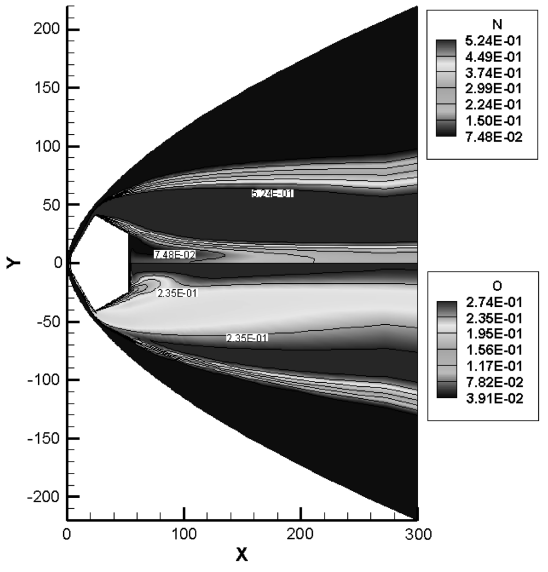

Fig. 3 Molar fraction of atoms N and O around the Stardust configuration; $u_\infty = 11.137$ km/s.

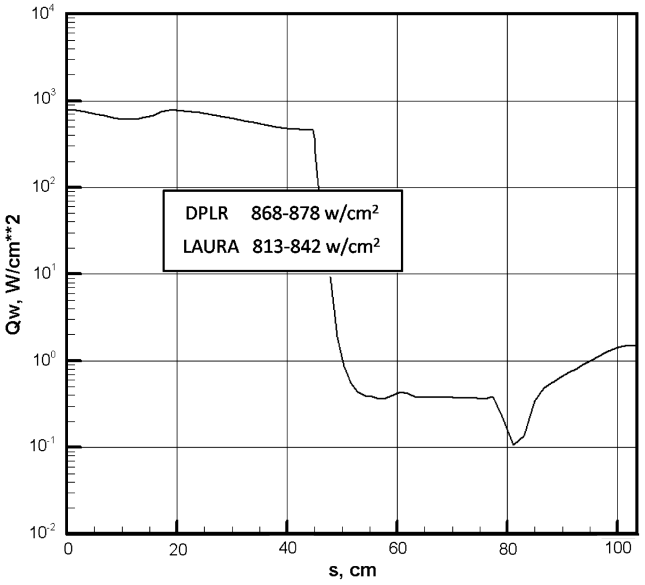

Fig. 4 Comparison of heat transfer on the symmetric plane of Stardust; $u_\infty = 11.137$ km/s.

depicted in Fig. 4. The heat transfer simulation is conducted at the peak heating reentry condition of the Stardust at the altitude of 59.77 km with the reentry speed of 11.137 km/s. At this condition, the freestream density and temperature are 2.43×10^{-4} kg/m^3 and 238.5 K. The present numerical results of maximum heat transfer to the surface of capsule agree very well with all numerical results generated by the two most widely adopted numerical procedures for thermal protection analyses: DPLR [33] and LAURA [34]. The heat transfer distribution along the capsule also agrees with the computational results in the open literature [10–12,16,17,33,34].

For lack of a validation database, the present results are considered comparable to all available computational results and will proceed to interpret the research findings. For the present purpose, the sum of conductive and convective heat transfer to the reentry configurations is chosen as the basis for predictive evaluation and supplemented by the comparison of the species concentration profile in the shock layer.

Translational–Vibrational Interaction Models

In describing nonequilibrium physical-chemical phenomena of energy transfer among internal degrees of freedom, the appropriate time scale remains as a principal hindrance. A part of the reason is that the energy-transfer process via collisions can take place in single (ladder climbing) or multiple quantum jumps (big bang) [26]. To overcome this difficult, Millikan and White [13] discover a linearly logarithmic relationship between the product of pressure and relaxation time scale to the inverse one-third power of system temperature, $\log(p\tau_v) \approx CT^{-1/3}$. Their remarkable correlation accurately describes the relaxation rates of vibrational excitation for a large group of gas species. Meanwhile, they also point out that at a sufficiently high-temperature condition for dissociation, this vibrational relaxation time scale may not be physically meaningful. Treanor and Marrone [14] specifically develop a CVD model to address this issue in which an exponential probability distribution for dissociation is introduced. In their formulation, the temperature for a nonequilibrium system is justified on the basis that more molecules are formed in the upper levels of the vibration excitation. Park [11,12], through his insight, solves the character-changing vibration relaxation of high-temperature gas from the Landau–Teller to diffusion type by a simple modification to the vibration temperature. His simple and ingenious approach includes the influence of the vibrational excitation to the rates of chemical reactions by a geometrical mean temperature of the translation and the vibration temperatures. His simple and practical approach has been adopted by nearly all engineering predictive analyses and appears to be satisfactory.

A direct comparative study between the model of Treanor–Marrone [14] and Park [11,12] seems to be desirable. To accomplish the stated objective, an assessment of different chemical kinetic models is depicted in Fig. 5. In this presentation, the comparisons are limited to the models of Olynick et al. [16] and Park [17] for carbonaceous surface without pyrolysis gas emission, and the computational results are focused on the conductive–convective heat transfer on the symmetric plane of the Stardust capsule. In these simulations, the reaction-rate constants for chemical reaction are based on the accumulative data by Park [11,12,17]. The negligible difference in the computed conductive–convective heat transfer rates between models is clear in evidence. The affinity in the stagnation and the corner of the capsule region is observed, and only a small difference is noted between the results in the upstream to the corner and in the base region. It may be concluded that the difference in the chemical kinetic models has been substantially eliminated by the sustained period of research in NASA.

Figure 6 presents the comparison of the kinetic models with translational and vibrational excitations that are derived from the works of Park [11,12] and Treanor–Marrone [14]. These two models have an entirely different conceptual origin: the former is by insight and experience, and the latter has a reasonably theoretic base. However, the computational results using these models for the Stardust capsule at the peak heating load produce nearly identical results. The computational results reveal less difference than that from the different chemical kinetic models for carbonaceous surface. The magnitude of the disparity between two models is just a fraction of 1%. The only meaningful conclusions can be drawn from the present computations are that 1) Park's insight for treating the vibrational relaxation is remarkable and 2) the perturbation of dissociation to vibration relaxation at the peak heat load condition of the Stardust capsule is relatively insignificant. Under this circumstance, multiple quantum transitions and exchange collisions may not be the dominant energy-transfer mechanisms.

Electronic Conservation Equation

The electronic energy conservation equation (5) contains the most uncertain and unverifiable assumptions for modeling. The energy transfers between translational–electronic, vibrational–electronic, and ion–electron collisions have a very wide and plausible group of formulations [11,12,16–23] and none of them can be validated through a reliable process. Adding to these uncertainties, the reaction-rate constants for ionizing impose an even greater number of unknowns. Even from the simulated flow around the Stardust, the

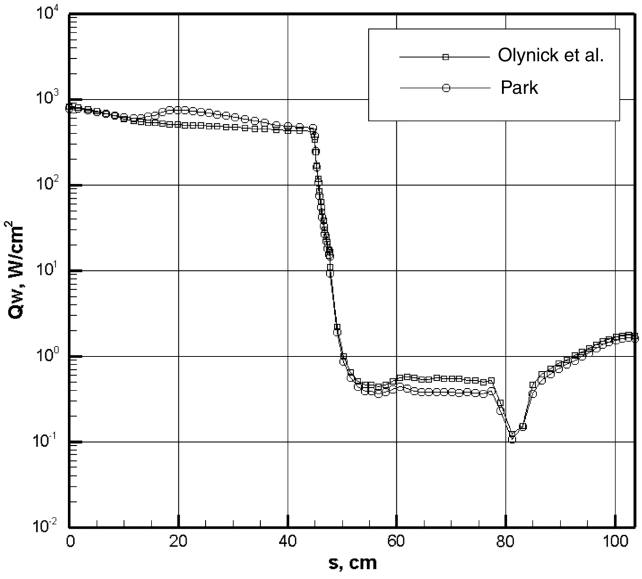

Fig. 5 Comparison of chemical kinetic models of Olynick et al. [16] and Park [17] for carbonaceous surface.

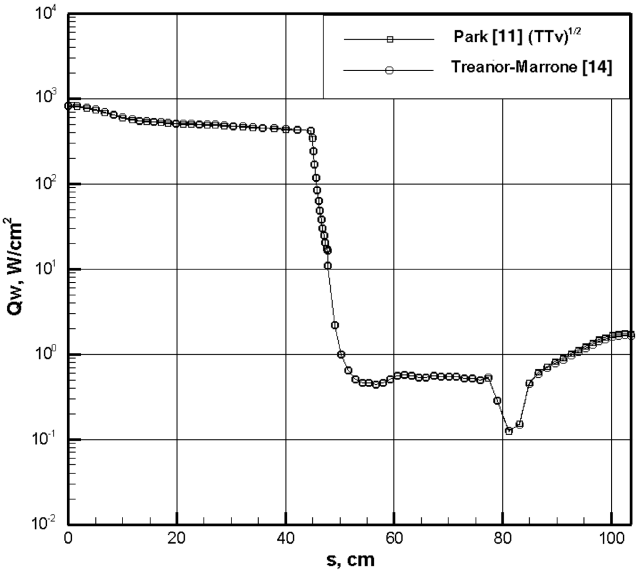

Fig. 6 Comparison of vibration–dissociation interaction models.

maximum electron temperature is 16,500 K and only exists in a very narrow domain shortly downstream of the bow shock.

In Fig. 7, a composite presentation includes the electronic temperature of the overall flowfield and an enlarged thin shock layer domain over the heat shield. The high electronic temperature only exists downstream to the relaxation zone away from the bow shock and rapidly disperses after the expansion over the outer edge of the heat shield. The calculated value is lower than the characteristic electronic temperatures of the first quantum level above the ground state for molecular nitrogen and nitro-oxide (50,000 K), atomic nitrogen (27,000 K), and atomic oxygen (22,700 K). The calculated electronic temperature is only greater than the molecular oxygen (11,300 K) [26]. Therefore, the shock layer of the Stardust capsule may not be densely populated with the gas mixture of the high quantum level far above the first electronic excited state. It may be further postulated that the amount of energy transfer to and from electronic excitation is mostly from the chemical kinetic process alone under this circumstance.

As was mentioned early in the present study, in the absence of the externally applied electric and magnetic fields, the electromagnetic force and energy of the partially ionized gas contribute very little to the total energy content during the reentry, but only alter the flow medium to become an electrically conducting material for electromagnetic wave propagation. This specific transport property can be determined by the existing chemical kinetic models [9,16,17]. From this viewpoint, it is questioned whether including the electronic energy conservation with the governing equations system for conductive–convective heat transfer is necessary, even at a reentry speed up to 12 km/s. The principal concern here is to minimize the number of uncertainties in the physical-chemical kinetic model for calculating the conductive and convective heat transfer.

As the first illustration of the present observation, the chemical compositions of the high-temperature gas, with and without the inclusion of the electronic energy conservation equation (5), within the shock layer of RAM-C-II along the stagnation streamline are given side by side in Fig. 8. The species composition is calculated for the probe at an altitude of 61 km at the freestream and surface temperature of 198.6 and 1500.0 K. The adopted chemical kinetic model is the 11-species and 32-elementary-reaction formulation by Park [11]. The supporting meshes for these computations are different: 105×51 and 75×25. The result of the reduced governing equations was conducted on a coarser mesh on the right-hand side of the graph; thus, the resolution of the shock standoff distance shows discrepancy, but the profiles of all pertaining species are nearly identical. The numerical results seem to indicate that the energy-transfer mechanism other than the chemical reaction is not dominant for the electronic excitation at this flight condition.

Figure 9 depicts a result similar to that of Fig. 8, but from the computational results of the Stardust capsule at the altitude of 59.79 km with a reentry speed of 11.14 km/s and the ambient temperature of 238.5 K. Two groups of species concentration profiles in molar fraction with and without the coupling of the electronic energy conservation equation are depicted side by side. The numerical results with the full complement of the governing equations are included in the right-hand side of this figure. The chemical kinetic model is based on the formulation of Olynick et al. [16] for carbonaceous surfaces. All calculations are conducted on the identical multiple-block grid with the dimensions of 31×41, 31×41, and 21×41. The two groups of the calculated species concentration are identical except for the tracing elements, such as C_3, HCN, and C^+ for the nonablating simulation. The magnitude of these species is less than 10^{-4} in molar fraction.

To further demonstrate the fact that the modeled energy transfer via the translation–electron and vibration–electron collisions and the energy cascading from electronic to vibrational excitation are not the dominant mechanisms of the chemical kinetic process at the simulated condition, the vibrational and electronic temperatures along the stagnation streamline of two different models are given by Fig. 10. In that figure, the temperatures of different internal degrees of excitations are calculated by assuming that the Boltzmann distributions are still applicable. The numerical results of the full complement of model equations are put on the right-hand side of the figure.

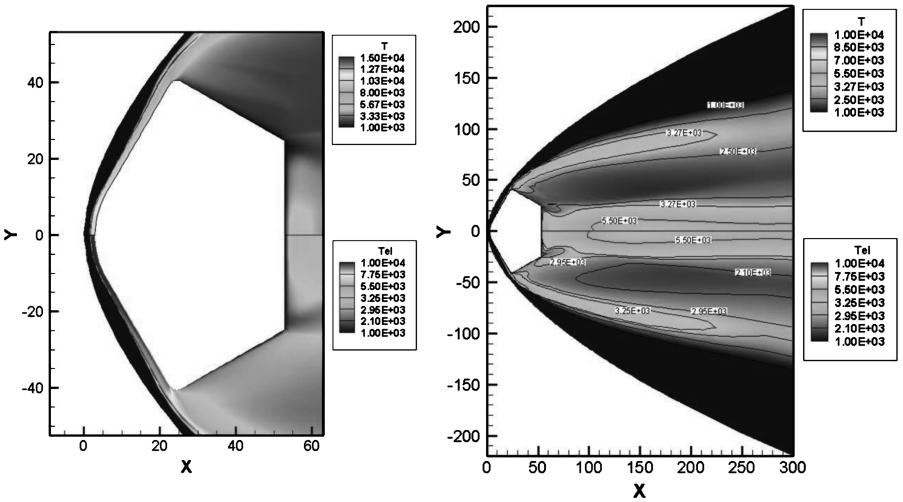

Fig. 7 Electronic temperature distribution within the shock layer of the Stardust capsule.

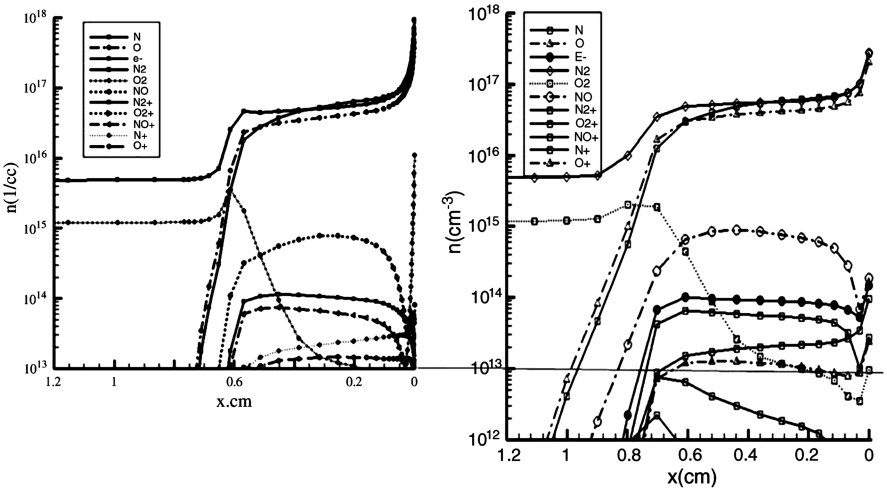

Fig. 8 Comparison of species concentration along the stagnation streamline of RAM-C-II; altitude is 61.0 km.

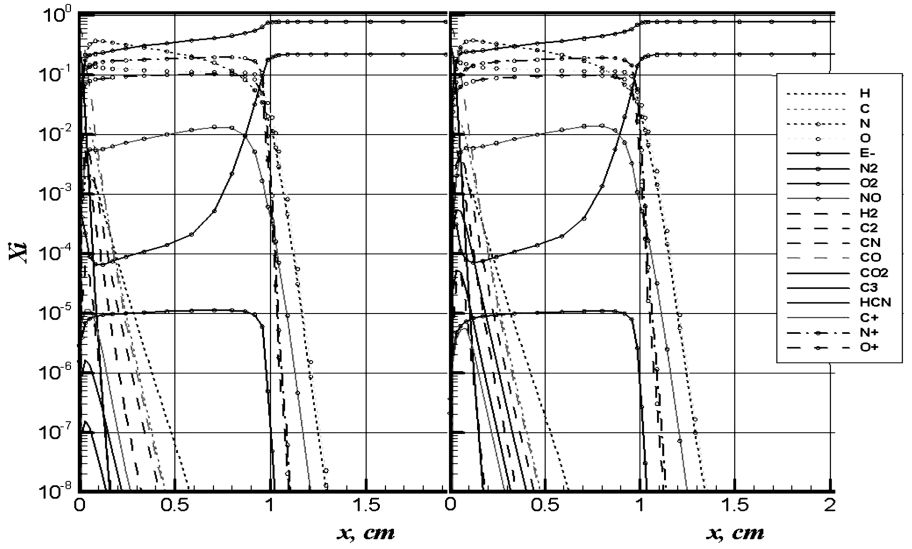

Fig. 9 Comparison of species concentration along the stagnation streamline of the Stardust capsule; altitude is 59.79 km.

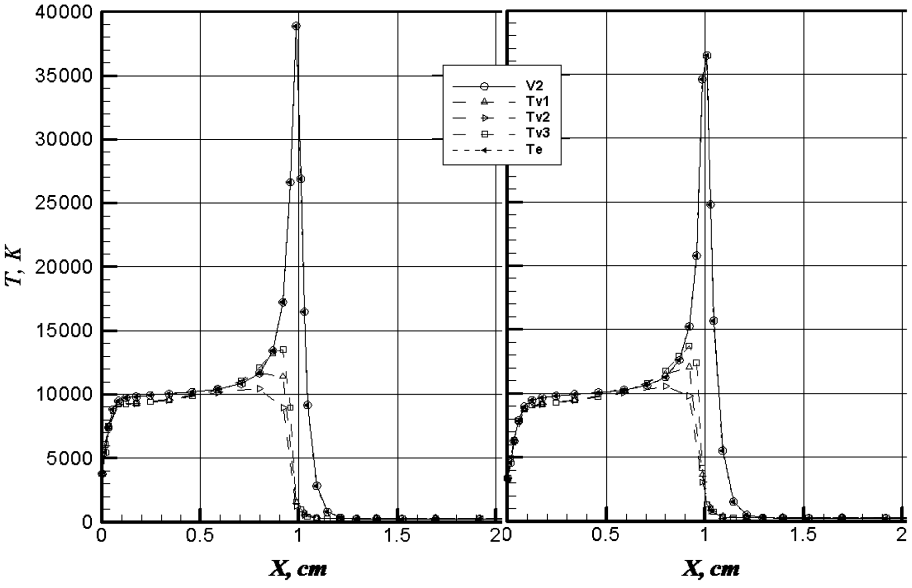

Fig. 10 Comparison of temperatures along the stagnation streamline of Stardust; altitude is 59.79 km.

The vibrational temperatures of O_2, N_2, and NO between two different models are essentially identical. The computed translational temperatures are bracketed between the values of 36,400 and 39,000 K to fall within the range of all known numerical results [16,17]. The lower translational temperature from the full complement of energy conservation equations correctly reflects the fact that a greater amount of energy is distributed to the electronic excitation. However, the difference in the predicted temperature is less than 7%, and there is no creditable verification by either experimental observation or theoretical analysis.

Figure 11 depicts the comparison of the computed conductive–convective heat transfer rates with and without the electronic energy conservative equation in the symmetric plane on the Stardust capsule. These compared computational results are obtained at the peak heat load condition. The reduced governing equations system eliminates the most energy-transfer mechanisms into the electronic excitation from lower internal degrees of excitation. As a consequence, the heat transfer rate is greater with the reduced model than with the full complement formulation. This difference is caused mainly by the increased conductive heat transfer at a higher translational temperature, but not from the nearly identical latent heat release from the recombined radicals on the surface. Under the condition without the emission of pyrolysis gas, the computed heat transfer rates are still within the scattering range of the results of Olynick et al. [16], Park [17], and all others that are generated from the computer programs based on DPLR [33] and LAURA [34]. The difference is noted only in the stagnation region and downstream to the corner of the forebody. However, the difference in the downstream domain is less significant in magnitude, but is exaggerated by the logarithmic plotting scale.

A critically important remark must be made regarding the electronic energy conservation equation: it is not the fact that the energy transfer to and from the electronic excitation is ignorable or that it does not have a profound influence to the nonequilibrium thermodynamic state of the reentry flow, but the uncertainty of the chemical kinetic models for electronic excitation diminish its value to be included it into the governing equation system. The simplified approximation saves more than 20% of the required computing resource. In short, additional and sustained research efforts are still needed to better understand the complex high-temperature physical-chemical phenomena for developing a more accurate modeling for numerical simulation.

Nonequilibrium Radiative Heat Transfer

In a hypersonic reentry environment, the radiation heat transfer generates a substantial amount of energy transfer in addition to the conductive and convective processes. In fact, at the maximum heat loading condition for the Stardust reentry, the radiation heat transfer rate is 120 w/cm^2 versus the convective–conductive heat transfer rate of 839 w/cm^2 [16,17]. Therefore, it is critically important to understand the basic mechanism and to develop the predictive methods. The high-temperature gas mixture in shock layers and wakes of entering space vehicles contains optically active components as CO_2, H_2O, CH_4, N_2, O_2, NO, N_2^+, C_2, CO, etc. The radiative heat transfer computation requires the development of effective numerical simulation methods, not only for prediction of spectral radiation fluxes inside the radiating volume, but also on the space vehicle surfaces.

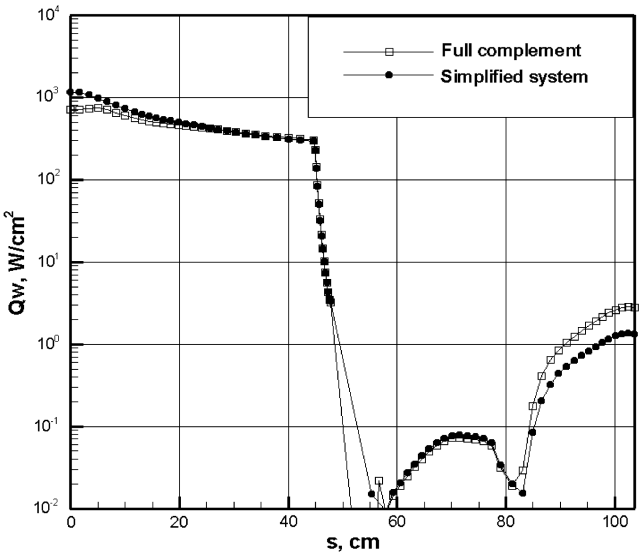

Fig. 11 Comparison of convective heat transfer on the symmetrical plane of Stardust; altitude is 59.79 km.

The energy propagating mechanism of the radiative heat transfer is fundamentally different from the convective or conductive process. It is a phenomenon associated with any quantum state jumps of molecule and atom, which has a spectrum from far infrared to near ultraviolet and beyond. Therefore, the electronic excitation is not ignorable in radiative calculation, in contrast to that in convective–conductive heat transfer simulation.

The multigroup, wideband, and narrowband spectra, as well as the line-by-line integration over a spectrum model of selective radiation heat transfer, are commonly used [35,36]. A detailed classification of different models, which are used in theory of radiation heat transfer, is presented in the work by Surzhikov et al. [35]. All these models use a similar computational algorithm: namely, an investigated spectral range is divided into finite spectral regions. Within each narrow spectral region, the equation of radiation heat transfer is solved by the frequency-independent spectral coefficients of emission and absorption. The integrated absorptivity (emissivity) in a full spectral range is determined by summation of integrated absorptivity (emissivity) in the separated frequency ranges. The average characteristics are then obtained by integrating the individual spectral group (spectral region) $\Delta\omega$. As expected, the computational efficiency of the models decreases with an increased number of spectral regions considered. The governing equation for radiation heat transfer can be given by the equation of spectral intensity for radiation:

$$\mathbf{\Omega}\,\frac{\partial \mathbf{J}_\omega(\mathbf{r},\mathbf{\Omega})}{\partial r} + \kappa_\omega(\mathbf{r})\mathbf{J}_\omega(\mathbf{r},\mathbf{\Omega}) = j_\omega(\mathbf{r}) \tag{11}$$

where $\mathbf{J}_\omega(\mathbf{r},\mathbf{\Omega})$ is the spectral intensity of heat radiation; $\kappa_\omega(\mathbf{r})$ is the spectral absorption coefficient; and $j_\omega(\mathbf{r})$ is the spectral emission coefficient, which can be calculated in the case of local thermodynamic equilibrium by the Kirchhoff law:

$$j_\omega(\mathbf{r}) = \kappa_\omega(\mathbf{r})J_{b,\omega}(\mathbf{r}) \tag{12}$$

The total radiation heat flux is obtained by integration over the radial $\mathbf{r}$ and solid angle $\mathbf{\Omega}$ through the full spectrum ω of the rotational line structure of diatomic and multi-atomic species:

$$q_r = \int_{4\pi} \mathrm{d}\Omega \int_{\Delta\omega_{\mathrm{tot}}} J_\omega(\mathbf{r},\mathbf{\Omega})\Omega\,\mathrm{d}r \tag{13}$$

The numerical simulation models have been integrated with computational fluid dynamic formulation for predicting aerothermodynamics of entering space vehicles [36]. To create a coupled multigroup spectral model, the initial conditions of the flowfield, including the temperature distributions and species concentration, were obtained from the governing equations for the nonequilibrium hypersonic flows [Eqs. (1–5)]. The radiation heat transfer is calculated by the half-moment method for radiation in one-dimensional approximation. The preliminary result of the incident spectral radiation heat fluxes at the stagnation region of a selected space vehicle [36,37] is presented in here. A group of four preliminary solutions is displayed for the spectral region of $1000 < \Delta\omega < 4000$ cm^{-1}. The progressive divisions of the spectral region by 10, 37, 500, and 100 groups are presented in Figs. 12a–12d.

The unique feature for the spectral group approach for analyzing the nonequilibrium radiation heat transfer is that the basic pattern of radiating fluxes can be captured by the sparse grouping of the

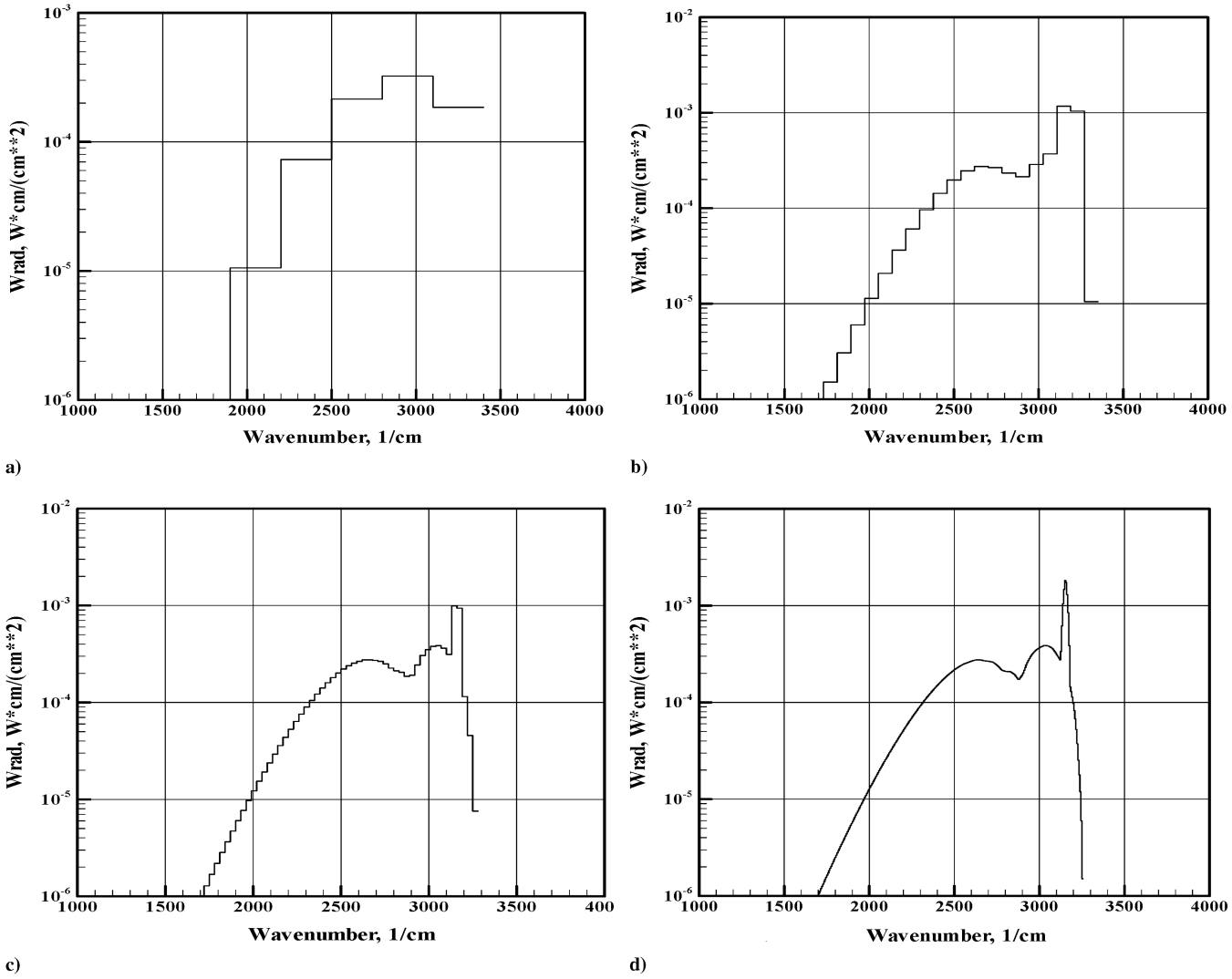

Fig. 12 Plots of divisions with a) 10 groups, b) 37 groups, c) 500 groups, and d) 100 groups.

spectrum. The definition is sharpened as the number of groups is refined. Another example of using the multigroup spectral approach has also applied to the Fire-II flight data [37] at higher and wider spectra from 1613 to 50, 015 cm^{-1}. This result will be presented in a future effort. It is noted that these radiative fluxes have a weak dependence on the spectral group number. Nevertheless, it should be stressed that the influence of spectral group number on radiation fluxes can be significant in other circumstances.

Conclusions

For the nonequilibrium hypersonic flow around the reentering Stardust capsule, the present investigation has found that the computed conductive–convective heat transfer rates are nearly identical with either Park's geometrical mean translational and vibrational temperature formulation or the dissociation preferential model by Treanor–Marrone. The predicted conductive–convective heat transfer rate for the reentering Stardust capsule is also found to be insensitive to whether the chemical kinetic models are implemented with and without the electronic energy conservation equations. However, it must be emphasized that this computational result is derived from the widely adopted, approximated chemical kinetic models for ionization and electronic excitation.

A preliminary nonequilibrium radiation computational procedure by a multigroup spectrum is also presented here as a simple illustration in the present stage of progress for developing a complete predictive capability for reentry simulation.

From our knowledge of high-temperature nonequilibrium hypersonic flow, the energy transfer among the internal degrees of freedom of high-temperature gas consists of two major mechanisms: energy transfer within the excited internal modes and the chemical kinetic processes. The processes are complex and our understanding of the physical-chemical interaction in the molecular and atomic scales is extremely limited, and the physical-chemical models have ample room for improvement.

Acknowledgments

The authors deeply appreciate the sponsorship by John Schmisseur of the U.S. Air Force Office of Scientific Research and the support by Donald Paul and Jose Camberos of the U.S. Air Force Research Laboratory.

References

[1] Milos, F., and Chen, Y., "Ablation and Thermal Response Property Model Validation for Phenolic Impregnated Carbon Ablator," AIAA Paper 2009-0262, Orlando FL, 2009.

[2] Chen, Y. K., and Milos, F. S., "Ablation and Thermal Response Program for Spacecraft Heatshield Analysis," *Journal of Spacecraft and Rockets*, Vol. 36, 1999, pp. 475–483. doi:10.2514/2.3469

[3] Koo, J. H., Ho, D., and Ezekoye, O., "A Review of Numerical and Experimental Characterization of Thermal Protection Materials—Part I., Numerical Modeling," AIAA Paper 2006-4936, July 2006.

[4] Torre, L., Kenny, J. M., and Maffezzoli, "Degradation Behavior of a Composite material for Thermal Protection System Part I—Experimental Characterization," *Journal of Material Science and Technology (Sofia)*, Vol. 33, No. 12, 1998, pp. 3137–3143.
[5] Sutton, G., "The Initial Development of Ablation Heat Protection: An Historical Perspective," *Journal of Spacecraft and Rockets*, Vol. 19, No. 1, 1982, pp. 3–11. doi:10.2514/3.62196
[6] Park, C., and Balakrishnan, A., "Ablation of Galileo Probe Heat-Shield Models in a Ballistic Range," *AIAA Journal*, Vol. 23, 1985, pp. 301–308. doi:10.2514/3.8910
[7] Chapman, S., and Cowling, T. G., *The Mathematical Theory of Nonuniform Gases*, Cambridge Univ. Press, New york, 1964, pp. 134–150.
[8] Park, C., "Stagnation-Point Ablation of Carbonaceous Flat Disk, Part 1: Theory," *AIAA Journal*, Vol. 21, No. 11, 1983, pp. 1588–1594. doi:10.2514/3.8293
[9] Zhluktov, S., and Abe, T., "Viscous Shock-layer Simulation of Air flow Past Ablating Blunt Body with Carbon Surface," *Journal of Thermophysics and Heat Transfer*, Vol. 13, No. 1, 1999, pp. 50–59. doi:10.2514/2.6400
[10] Chen, Y. K., and Milo, F. S., "Navier-Stokes Solutions with Finite Rate Ablation for Planetary Mission Earth Mission Earth Reentries," *Journal of Spacecraft and Rockets*, Vol. 42, No. 6, 2005, pp. 961–970. doi:10.2514/1.12248
[11] Park, C., "Review of Chemical Kinetics Problems of Future NASA Missions, I Earth Entries," *Journal of Thermophysics and Heat Transfer*, Vol. 7, No. 3, 1993, pp. 385–398. doi:10.2514/3.431
[12] Park, C., "Chemical-Kinetic Parameters of Hypersonic Earth Entry," *Journal of Thermophysics and Heat Transfer*, Vol. 15, No. 1, 2001, pp. 76–90. doi:10.2514/2.6582
[13] Millikan, R. C., and White, D. R., "Systematics of Vibrational Relaxation," *Journal of Chemical Physics*, Vol. 39, No. 12, 1963, pp. 3209–3213. doi:10.1063/1.1734182
[14] Treanor, C. E., and Marrone, P. V., "Effect of Dissociation on the Rate of Vibrational Relaxation," *Physics of Fluids*, Vol. 5, No. 9, 1962, pp. 1022–1026. doi:10.1063/1.1724467
[15] Willcockson, W. H., "Stardust Sample Return Capsule Design Experience," *Journal of Spacecraft and Rockets*, Vol. 36, No. 3, 1999, pp. 470–474. doi:10.2514/2.3468
[16] Olynick, D. R., Chen, Y. K., and Tauber, M. E., "Aerodynamics of the Stardust Sample Return Capsule," *Journal of Spacecraft and Rockets*, Vol. 36, No. 3, 1999, pp. 442–462. doi:10.2514/2.3466
[17] Park, C., "Calculation of Stagnation-Point Heating Rates Associated with Stardust Vehicle," *Journal of Spacecraft and Rockets*, Vol. 44, No. 1, 2007, pp. 24–32. doi:10.2514/1.15745
[18] Surzhikov, S. T., Sharikov, I. V., Capitelli, M., and Colonna G., "Kinetic Models of Nonequilibrium Radiation of Strong Air Shock Waves," AIAA Paper 2006-0586, 2006.
[19] Lee, J. H., "Basic Governing Equations for the Flight Regime of Aeroassisted Orbital Transfer Vehicles," *Progress in Aeronautics and Astronautics: Thermal Design of Aeroassisted Orbital Transfer Vehicles*, Vol. 96, AIAA, New York, NY, 1985, pp. 3–53.
[20] Candler, G. V., and MacCormack, R. W., "Computation of Weakly Ionized Hypersonic Flows in Thermochemical Nonequilibrium," *Journal of Thermophysics and Heat Transfer*, Vol. 5, No. 3, 1991, pp. 266–272. doi:10.2514/3.260
[21] Surzhikov, S. T., and Shang, J. S., "Kinetics Models Analysis for Super-Orbital Aerophysics," AIAA Paper 2008-1278, Reno NV, 2008.
[22] Shang, J. S., Surzhikov, S. T., and Yan, H., "Simulating Hypersonic Nonequilibrium Flow Using Kinetic Models," AIAA Paper 2009-0286, Orland FL, 2009.
[23] Shang, J. S., "Analysis of Hypersonic Nonequilibrium Flow over Ablating Surface," AIAA Paper 2009-4051, San Antonio TX, 2009.
[24] Grasso, F., and Capano, G., "Modeling of Ionizing Hypersonic Flows in Nonequilibrium," *Journal of Spacecraft and Rockets*, Vol. 32, 1995, pp. 217–224. doi:10.2514/3.26599
[25] Josyula, E., and Bailey, W. F., "Governing Equations for Weakly Ionized Plasma Flow field of Aerospace Vehicles," *Journal of Spacecraft and Rockets*, Vol. 40, No. 6, 2003, pp. 845–857. doi:10.2514/2.7036
[26] Clarke, J. F., and McChesney, M., *The Dynamics of Real Gases*, Butterworth, Washington, D. C., 1964, pp. 66–86.
[27] Surzhikov, S. T., "Radiative-Gasdynamics Model of a Martian Space Vehicle," AIAA Paper 2004-1355, 2004.
[28] Capitelli, M., Gorse, C., Longo, S., and Giordano, D., "Collision Integrals of High-Temperature Air Species," *Journal of Thermophysics and Heat Transfer*, Vol. 14, No. 2, 2000, pp. 259–268. doi:10.2514/2.6517
[29] Levin, E., and Wright, M. J., "Collision Integrals for Ion-Neutral Interactions of Nitrogen and Oxygen," *Journal of Thermophysics and Heat Transfer*, Vol. 18, No. 1, 2004, pp. 143–147. doi:10.2514/1.2552
[30] Svehla, R. A., "Estimated Viscosities and Thermal Conductivities of Gases at High Temperatures," NASA TR-R-132, 1962.
[31] Bird, R. B., Stewart, W. E., and Lightfoot, E. N., *Transport Phenomenon*, 2nd ed., Wiley, New York, 2002, pp. 25, 274, 526.
[32] Jones, L. J., and Cross, A. E., "Electrostatic Probe Measurements of Plasma Parameters for Two Reentry Flight Experiments at 25,000 feet per Second," NASA TN D 66-17, 1972.
[33] Wright, M. J., Candler, G. V., and Bose, D., "Data-Parallel Line Relaxation Method for the Navier-Stokes Equations," *AIAA Journal*, Vol. 36, Sept. 1998, pp. 1603–1609. doi:10.2514/2.586
[34] Cheatwood, F., and Gnoffo, P., "User's Manual for the Langley Aerothermodynamic Upwind Relaxation Algorithm (LAURA)," NASA TM 4674, April 1996.
[35] Surzhikov, S. T., Sharikov, I. V., Capitelli, M., and Colonna, G., "Kinetic Models of Nonequilibrium Radiation of Strong Air Shock Waves," AIAA Paper 2006-0586, 2006.
[36] Surzhikov, S. T., "Computing System for Solving Radiative Gasdynamic Problems of Entry and Re-Entry Space Vehicles," *Proceedings of the International Workshop on Radiation of High Temperature Gases in Atmospheric Entry*, SP-533, ESA, 8–10 Oct. 2003, pp. 111–117.
[37] Olynick, D. R., Henline, W. D., Chambers, L. H., and Candler, G. V., "Comparison of Coupled Radiative Navier-Stokes Flow Solutions with the Project Fire-II Flight Data," AIAA Paper 94-1955, 1995.

G. Palmer
Associate Editor